More recently, we have identified novel variants for *EML4-ALK* fusion gene with cDNA screening and multiplex reverse transcription-polymerase chain reaction (RT-PCR), capturing all possible in-frame fusions of *EML4* to exon 20 of *ALK*. By carrying out cDNA screening, we identified variant 3,[8] and using multiplex RT-PCR assays, we identified variants 4 and 5[9] after the first identification of variants 1 and 2. In variant 3, exon 6 of *EML4* is joined to exon 20 of *ALK*. cDNA from variant 4 ligates exon 14 of *EML4* to a position within exon 20 of *ALK*, whereas another cDNA from a variant 5 tumor connects exon 2 of *EML4* to exon 20 of *ALK*. All the new three isoforms of *EML4-ALK* have a marked oncogenic activity *in vitro* as well as *in vivo*.[8,9] The variant 3 was also identified by Rikova *et al*[10] and another new variant, in which exon 15 of *EML4* is jointed to a position within exon 20 of *ALK*, was identified by Koivunen *et al*.[11]

Earlier we conducted the first large scale-study to detect *EML4-ALK* (3.4%) in lung adenocarcinomas and found five fusion-positive cases (two variant 1 and three variant 2) in 149 adenocarcinoma samples.[12] At that point in time, only two variants were recognized, and we investigated their clinicopathological characteristics. However, with development of multiplex RT-PCR for detecting all possible in-frame variants, we captured theoretically all *EML4-ALK* variants and found 11 *EML4-ALK*-positive cases among 363 lung cancers.[9] In this study, we examined the clinicopathological and genetic features of the 11 tumors, and found *EML4-ALK* lung cancers to be characterized by a lack of *EGFR* and *KRAS* mutations, a low rate for *TP53* mutations, a thyroid transcription factor-1 (TTF-1)-positive cell lineage, an acinar histology, and young onset.

Materials and methods

Clinical Samples and Pathological Review

The clinical specimens for this study were 11 lung tumors detected in our earlier study, using multiplex RT-PCR and fluorescent *in situ* hybridization.[9] Briefly, samples were obtained from 363 individuals who underwent surgery at the Cancer Institute Hospital (Tokyo, Japan) between May 1997 and February 2004. The 363 lung cancers comprised 253 adenocarcinomas, 7 adenosquamous carcinomas, 72 squamous cell carcinomas, 7 large-cell carcinomas (including 4 large-cell neuroendocrine carcinomas), 2 pleomorphic carcinomas, and 22 small-cell carcinomas. This project was approved by the Institutional Review Board of the Japanese Foundation for Cancer Research, and informed consent was obtained from each study subject. Histological diagnoses were made based on the World Health Organization (WHO) classification.[13] However, with its subdivision of lung adenocarcinomas, more than 80% tumors fell into the mixed subtype category. We therefore additionally used a predominance classification of invasive components, which is mostly based on the WHO classification except for the mixed subtype, such as papillary predominant, acinar predominant, etc. In the predominance classification of invasive components, we diagnose by a component that makes up the predominant portion of invasive lesion even if it is <50%. In addition, we used a differentiation grading that was basically according to the former version of the Japanese Lung Cancer Society criteria,[14] as performed earlier.[15]

Immunohistochemical Analysis

Unstained paraffin-embedded sections were depleted of paraffin with xylene, rehydrated through a graded series of ethanol solutions, and subjected to immunohistochemical staining with a mouse monoclonal antibody (ALK1, 1:20, Dako, Carpinteria, CA, USA). Heat-induced antigen retrieval pretreatment was performed with Target Retrieval Solution pH 9.0 (Dako). Immune complexes were detected with the EnVision+DAB system (Dako) with minor modifications.[16] TTF-1 was also immunostained using a mouse monoclonal antibody (clone 8G7G3/1, 1:100, Dako), as described earlier.[15] Tumors were considered negative if staining was found in <5% of neoplastic cells, partly positive if present in 5–50%, and positive if in more than 50%. The results of immunostaining with TTF-1 were based on nuclear staining of neoplastic cells.

DNA Extraction and Mutation Analysis of *EGFR*, *KRAS*, and *TP53*

Of 253 patients with adenocarcinomas, both *EGFR* and *KRAS* data were available for 68 patients and *EGFR* data alone for further 12 patients, including all the patients with *EML4-ALK*-positve cases.[12,17] DNA extraction and mutation analysis of *EGFR* and *KRAS* were performed as described earlier.[17] Mutation analysis of *TP53* was also performed as described earlier.[18] Genomic DNAs from fresh tumor samples were prepared and exons 4–8 and 10 of the *TP53* gene were analyzed by the PCR – single-strand conformation polymorphism and DNA sequencing. For case #4808, *TP53* mutation analysis was performed using DNA extracted from formalin-fixed paraffin-embedded tissue and a method based on direct sequencing, because no fresh sample was available for this study at the time of the current study.

Results

Histologically, the 253 adenocarcinomas comprised 213 mixed subtypes, 19 acinar, 9 papillary, 4 solid, 1 other, and 7 bronchioloalveolar carcinomas based on the WHO classification. According to the subdivision

of lung adenocarcinomas with the WHO criteria, more than 80% of tumors fell into the mixed subtype category. However, this contains very varied lesions; for example, a tumor comprising solid and acinar adenocarcinoma elements would be expected to have a very different prognosis from one composed of bronchioloalveolar carcinoma, with only a small amount of papillary adenocarcinoma. We therefore additionally used a predominance classification and also paid attention to the minor components. According to the predominance subtypes in adenocarcinomas, 6 of 11 *EML4-ALK*-positive lung cancers (54.5%) were subclassified as acinar adenocarcinomas ($P=0.000044$, Table 1), as compared with 4 based on the WHO classification (36.4%, $P=0.0018$, Table 2). In other words, 6 of 34 (18%) acinar-predominant adenocarcinomas, as well as 4 of 19 (21%) acinar adenocarcinomas based on the WHO classification, have *EML4-ALK* fusion. In adenocarcinomas not subclassified as acinar adenocarcinomas based on the WHO criteria, acinar structures were also frequently observed (Figure 1). In differentiation grading, *EML4-ALK* lung cancers were less differentiated (Table 3, $P=0.0082$, 10/11). In addition, they often featured mucin production, as proven by Alcian Blue staining (Figure 1b) with acinar structures. As for the cell types originally proposed by Hashimoto *et al*,[18] the columnar cell type was characteristic of *EML4-ALK* lung cancers (Figure 1).

EML4-ALK-positive lung adenocarcinomas were also found to be significantly smaller than other lung adenocarcinomas (Table 3, $P=0.031$), in line with the lack of bronchioloalveolar components.

Patients with *EML4-ALK* lung cancers tended to be young (56 *vs* 64 years for other tumor types, $P=0.0062$). We defined early-onset lung cancers by classifying patients as below or above 50 years of age. In 253 patients with lung adenocarcinomas, 16 patients were affected by the disease at below 50 years of age. Four of 11 patients (36%) with *EML4-ALK*-positive lung cancers were affected by these diseases at below 50 years of age, as compared with 12 of 242 patients (5.0%) with *EML4-ALK*-negative lung cancers ($P=0.00038$).

It is true that the *EML4-ALK* translocation was first found in a smoker's lung cancer, but overall there was no significant difference between smokers' and non-smokers' tumors with regard to *EML4-ALK* fusion ($P=0.37$). Smoking habits can be classified into the following two grades of cumulative smoking based on the smoking index (SI), a product of the number of cigarettes per day, and the duration in years: (a) non-smokers and light smokers (SI <400); and (b) heavy smokers (SI $=400$ or above). Ten of the 11 (91%) *EML4-ALK*-positive lung cancer patients had SI <400, as compared with 109 of 241 (45%) *EML4-ALK*-negative lung cancer patients ($P=0.040$). In this study, *EML4-ALK* fusion was detected in only one heavy smoker's lung cancer (1/11 = 9.1%).

EGFR and *KRAS* mutations are mutually exclusive in usual cases while being two major oncogenic drivers of lung adenocarcinoma development. *EML4-ALK*-positive lung cancers lacked both *EGFR* and *KRAS* mutations ($P=0.00018$), and only 1 of 11 (9.1%) harbored a *TP53* mutation (Table 2). It is noteworthy that the single mutation was a G/A transition (GTG→ATG) (V→M) in codon 273, exon 8. This is known to be a spontaneous rather than a tobacco-carcinogen-induced mutation, usually seen in non-smokers' lung cancers.

In the *EML4-ALK*-positive 11 cases, immunohistochemical assays with the anti-ALK antibody ALK1 consistently showed definite staining. As illustrated

Table 1 *EML4-ALK* fusion and histology of adenocarcinomas classified by predominant subtypes

Histology	*Total (363)*	*EML4-ALK(+)*	*EML4-ALK(−)*
Adenocarcinoma	253	11 (4.3%)	242 (96%)
Subtype by predominance classification			
Invasive carcinoma			
Papillary adenocarcinoma	206	5 (5/11 = 45%)	201 (201/242 = 83%)
Acinar adenocarcinoma	34	6 (6/11 = 55%)[a]	28 (28/242 = 12%)
Solid adenocarcinoma with mucin	5	0 (0%)	5 (5/242 = 2.1%)
Others	1	0 (0%)	1 (1/242 = 0.41%)
Noninvasive carcinoma			
Bronchioloalveolar carcinoma	7	0 (0%)	7 (7/242 = 2.9%)
Adenosquamous carcinoma	7	0 (0%)	7 (100%)
Squamous cell carcinoma	72	0 (0%)	72 (100%)
Large-cell carcinoma	7	0 (0%)	7 (100%)
Large-cell neuroendocrine carcinoma	4	0 (0%)	4 (100%)
Pleomorphic carcinoma	2	0 (0%)	2 (100%)
Small-cell carcinoma	22	0 (0%)	22 (100%)

Acinar-predominant adenocarcinomas *vs* the other adenocarcinomas.
[a]Fisher's exact test, $P<0.0001$ ($P=0.000044$).

Table 2 *EML4-ALK* variants detected by multiplex RT-PCR analysis and clinicopathologic and genetic data

V	*Tumor ID*	*Sex*	*Age (years)*	*p-Stage*	*LKD*	*Survival (days)*	*Size (mm)*	*SI*	*WHO subtype*	*Pred-subtype*	*diff.*	*Histological components*	*ALK IHC*	*TTF-1 IHC*	*KRAS mut*	*EGFR mut*	*TP53 mut*
1	#9034	F	43	IA	Alive	1714	12	10	Acinar	Acinar	Por		+	P+	–	–	–
1	#4808	F	58	IA	Alive	2246	27	0	Mixed	Pap	Well	Papillary adenocarcinoma with BAC	+	+	–	–	–
1	#9968	F	66	IIIA	Alive	1036	33	0	Mixed	Pap	Mod	Papillary adenocarcinoma with BAC	+	+	–	–	–
2	#4180	M	43	IV	Dead	527	23	160	Acinar	Acinar	Por		+	P+	–	–	–
2	#3121	M	64	IIIB	Alive	2673	18	220	Acinar	Acinar	Por		+	+	–	–	–
2	#2374	F	66	IA	Alive	1632	28	0	Acinar	Acinar	Mod		+	P+	–	–	–
3	#7969	M	47	IIIA	Alive	1328	17	540	Mixed	Pap	Por	Papillary adenocarcinoma with BAC	+	+	–	–	–
3	#2075	F	62	IIA	Dead	522	19	0	Mixed	Acinar	Mod	Acinar+papillary+solid adenocarcinoma	+	P+	–	–	+[a]
3	#9616	M	73	IA	Alive	1465	13	300	Pap	Pap	Mod		+	+	–	–	–
4	#8398	F	52	IA	Alive	1834	24	0	Mixed	Acinar	Mod	Acinar+papillary adenocarcinoma with BAC	+	P+	–	–	–
5	#8893	M	44	IA	Alive	1730	15	0	Pap	Pap	Mod		+	+	–	–	–

acinar, acinar adenocarcinoma; BAC, bronchioloalveolar carcinoma; diff., differentiation; *EGFR* mut, *EGFR* mutation; IHC, immunohistochemistry; *KRAS* mut, *KRAS* mutation; LKD, lung cancer death; mixed, adenocarcinoma with mixed subtype; P+, Partly +; pap, papillary adenocarcinoma; Pred-subtype, predominance subtype; p-Stage, pathological-Stage; SI, smoking index; *TP53* mut, *TP53* mutation; V, *EML4-ALK* variant.

[a]G/A transition (GTG→ATG) (V→M) in codon 273, exon 8.

in Figure 2a, the cytoplasm of tumor cells harboring the variant 2 (tumor ID #2374) was strongly stained with fine granular accentuation. Although we performed the immunostaining of 88 *EML4-ALK*-negative lung adenocarcinoma specimens, we could discriminate all the fusion-negative specimens from the fusion-positive ones by our refined immunohistochemical condition.[16] All the 11 cases were also positive (six cases) or partly positive (five cases) for TTF-1 immunohistochemistry (Figure 2b), a characteristic of alveolar type II cells, which is featured in non-smokers' cancers.

Discussion

With the present large-scale screen for *EML4-ALK* fusion in lung cancers, we detected 11 adenocarcinomas with an *EML4-ALK* translocation. In the current study, we revealed a relatively young occurrence and a typically less-differentiated acinar histology, which might be used as clinical pointers. It is of great interest that *EML4-ALK* translocation is associated with young onset, whereas *EGFR* mutation status is not associated with the patient's age at diagnosis.[4]

Currently, anaplastic large-cell lymphomas (ALCLs) are divided into three entities, namely primary systemic *ALK* (+) ALCL, primary systemic *ALK* (−) ALCL, and primary cutaneous ALCL. The ALK expression is caused most commonly t(2;5) by chromosomal translocations, and *ALK* (+) ALCL predominantly affects young male patients and, if treated with chemotherapy, has a favorable prognosis.[19] This might similarly be applicable to *EML4-ALK* lung cancers. Presently, the primary treatment for lung cancers is surgery where possible. However, for *EML4-ALK* lung cancers, chemotherapy or a targeted therapy with an ALK inhibitor might be effective, given that *EML4-ALK*-dependent cells are known to undergo apoptosis in response.[7–9,11]

Here, *EML4-ALK* fusion was found to be mutually exclusive for *EGFR* or *KRAS* mutations, thus pointing to a distinct genetic subtype of lung adenocarcinoma. The possibility of a genetic classification of lung adenocarcinomas based on oncogene mutations has already been considered. In fact, one-third to nearly half of Japanese adenocarcinomas harbor *EGFR* mutations,[4,20] about 10% have *KRAS* mutations[21–23] and about 4% have *EML4-ALK* translocations, implying that two-thirds of adenocarcinomas feature mutually exclusive oncogenic mutations. The mutation rate of *TP53* (1/11 = 9.1%) was also low compared with that of lung adenocarcinomas in general (41%),[18] and the single mutation found was G to A transition, which was not related to smoking. Strong *in vitro* as well as *in vivo* oncogenic activity of *EML4-ALK* fusion products[8,9] might account for the lack of other genetic alterations.

All 11 *EML4-ALK* lung cancers were positive or partly positive for TTF-1 immunostaining. TTF-1

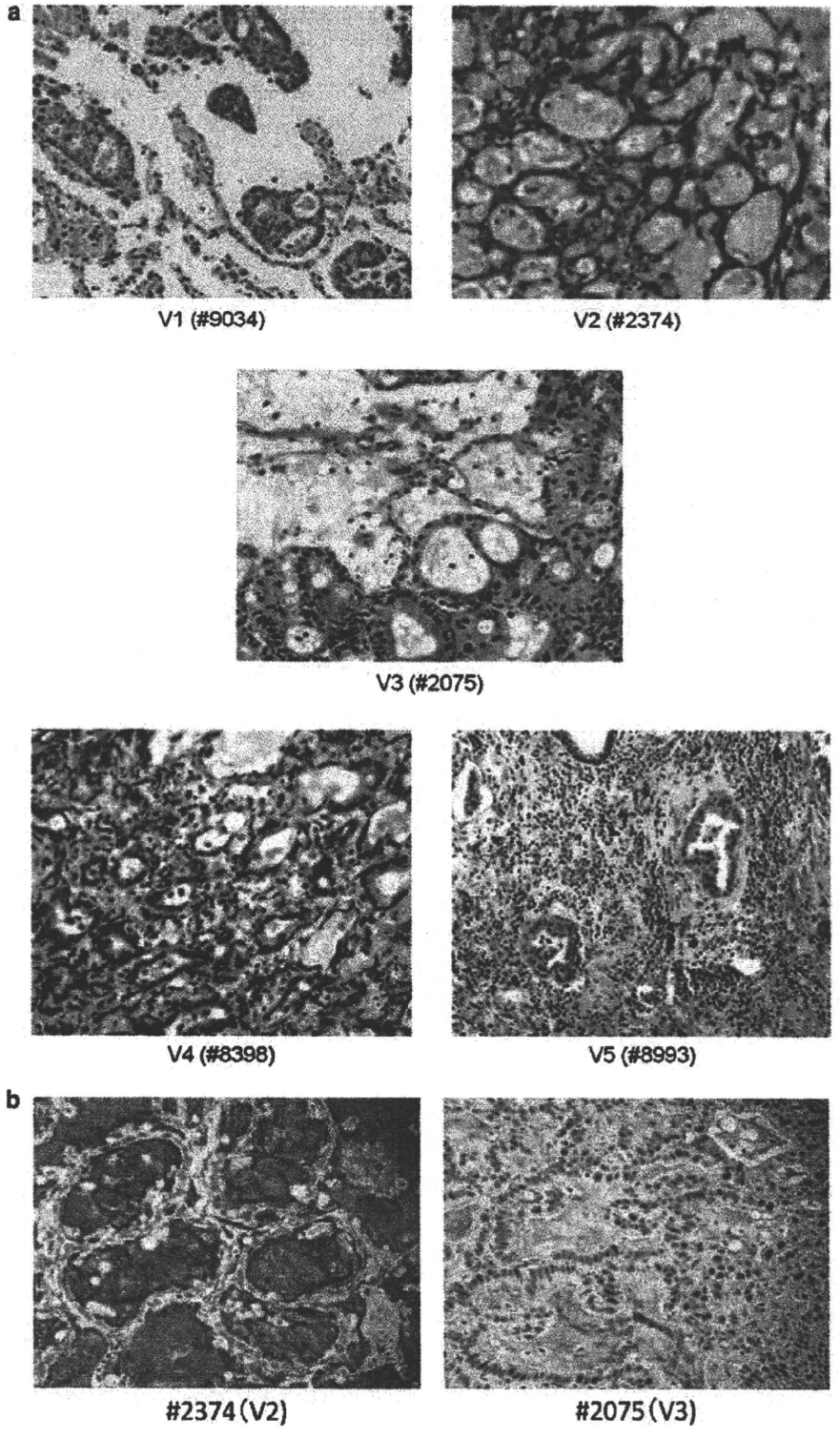

Figure 1 (**a**) Representative appearance of all the five variants of the *EML4-ALK* lung cancers (hematoxylin and eosin staining). Histologically, acinar structures with some mucin production are characteristic. (**b**) Alcian Blue staining shows the abundant mucin production.

Table 3 Clinicopathologic and genetic comparisons between *EML4-ALK* fusion-positive and -negative lung adenocarcinomas

Variables category	*No. of samples (%)*	*EML4-ALK fusion*		*P-value*
		(+) (n = *11*)	*(−)* (n = *242*)	
Age (years; mean ± s.d.)	253	56 ± 11	64 ± 9	0.0062[a] 0.00038[b]
<50	16 (6.3)	4 (36)	12 (5.0)	
≤50	237 (94)	7 (64)	230 (95)	
Sex				0.61[b]
Males	134 (53)	5 (45)	129 (53)	
Females	119 (47)	6 (55)	113 (47)	
Smoking habit				0.37[b]
Never smokers	105 (41)	6 (55)	99 (41)	
Ever smokers	147 (59)	5 (45)	142 (59)	
Heavy smokers or not				0.040[b]
Heavy smokers	110 (44)	1 (9.1)	109 (45)	
Not heavy smokers	142 (56)	10 (91)	132 (55)	
Tumor size (mm)		20.8 ± 6.7	31.8 ± 16.7	0.031[a] 0.039[b]
<30	142 (56)	10 (80)	132 (55)	
≥30	111 (44)	1 (20)	110 (45)	
Differentiation grading				0.0082[b]
Well	98 (39)	1 (9.1)	97 (40)	
Less	155 (39)	10 (91)	145 (60)	
EGFR mutation				0.00085[b]
Mutation(+)	41 (52)	0 (0)	41 (60)	
Mutation(−)	39 (48)	11 (100)	28 (40)	
KRAS mutation				0.49[b]
Mutation(+)	7 (10)	0 (0)	7 (12)	
Mutation(−)	61 (90)	11 (100)	50 (88)	
EGFR or *KRAS mutation*				0.00018[b]
Mutation(+)	38 (59)	0 (0)	38 (67)	
Mutation(−)	30 (41)	11 (100)	19 (33)	
p-Stage				0.89[b]
I	143 (57)	6 (55)	137 (57)	
II–IV	110 (43)	5 (45)	105 (43)	

Percentages may not total 100, because of rounding.
We have no smoking history of one patient.
Smoking habits were classified into the following two grades based on the smoking index: (a) non-smokers and light smokers (smoking index <400); and (b) heavy smokers (smoking index = 400 or above).
[a]Student's *t*-test.
[b]Fisher's exact test.

has a decisive role as a master regulatory transcription factor in lung development and in maintenance of the functions of terminal respiratory unit (TRU) cells.[24] The TTF-1 positivity of *EML4-ALK* lung cancers suggests that this subtype might have a TRU histogenesis. TRU-type lung cancers with a TTF-1-positive cell lineage often occur in non- or light smokers, which frequently harbor *EGFR* mutations (61%) and have less-frequent *TP53* mutations (36%) as compared with non-TRU-types (57%).[22] *EML4-ALK* lung cancers also occur in non- or light smokers but do not harbor *EGFR* mutations. The low frequency of *TP53* mutations (9.1%) not only indicates strong oncogenic activity for *EML4-ALK* fusion products but also suggests an independence from smoking, because smoker's adenocarcinomas very frequently harbor *TP53* mutations.[18]

Histologically, less-differentiated acinar structures composed of columnar cells appear characteristic of *EML4-ALK* lung adenocarcinomas. Generally, the columnar cell type is also found in smoker's lung adenocarcinomas, whereas the hobnail cell type, characterized by cytoplasmic protrusions and with a tadpole shape, is often observed in non-smoker's lung adenocarcinomas.[18] Although *EML4-ALK* lung cancers are TTF-1-positive, their histology is

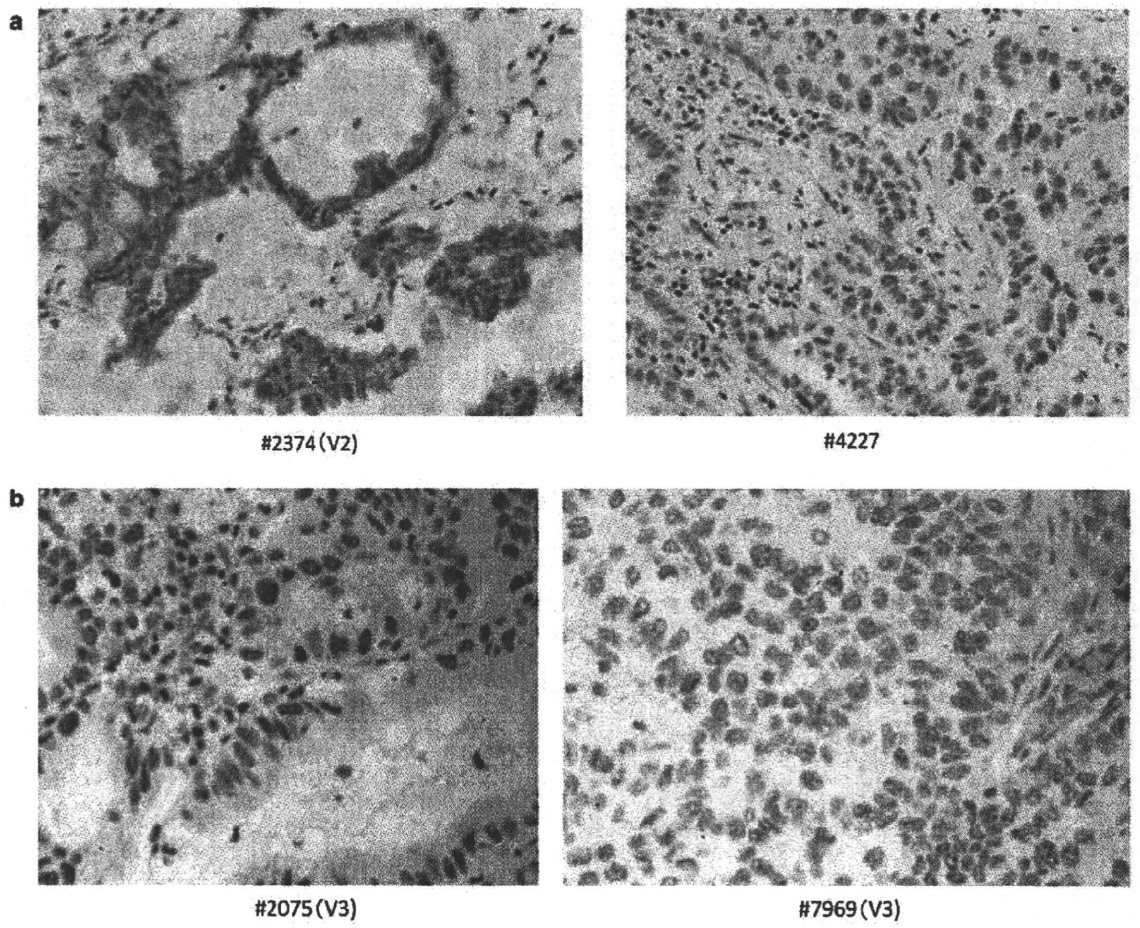

Figure 2 (**a**) Immunohistochemical analysis with a monoclonal anti-ALK antibody of lung adenocarcinoma specimens with (tumor ID #2374) and without (tumor ID #4227) *EML4-ALK* fusion. Note the diffuse staining in the cytoplasm with fine granular accentuation apparent for the *EML4-ALK*-positive tumor. (**b**) Immunohistochemical analysis of lung adenocarcinoma specimens with *EML4-ALK* fusion using a monoclonal anti-TTF-1 antibody. The *EML4-ALK*-positive tumors are partly (ID #2075) or diffusely (ID #7969) positive.

similar to lung cancers developing in smokers, which is interesting in the view of histology–etiology relationships.

Presently, lung adenocarcinomas may be genetically divided into *EGFR*-mutated, *KRAS*-mutated, and *EML4-ALK*-related subtypes. We here elucidated the clinicopathologic, histologic, and genetic characteristics of *EML4-ALK* lung cancers, bearing etiologic implications in mind. Just as some *EGFR*-mutated lung cancers can be successfully treated with EGFR inhibitors, *EML4-ALK* lung cancers may respond to a specific inhibitor treatment, allowing a good prognosis.

Acknowledgement

The authors thank Dr Malcolm Moore for the English correction of the manuscript, and Ms Kazuko Yokokawa, Mr Motoyoshi Iwakoshi, Ms Miyuki Kogure, and Ms Tomoyo Kakita for their technical assistance, and Ms Yuki Takano for her secretarial work. Parts of this study were supported financially by Grants-in-Aid for Scientific Research from the Ministry of Education, Culture, Sports, Science and Technology, from the Japan Society for the Promotion of Science, and by grants from the Ministry of Health, Labour and Welfare, the Smoking Research Foundation, the National Institute of Biomedical Innovation, and the Vehicle Racing Commemorative Foundation, as well as a Grant-in-Aid for Young Scientists (B).

Conflict of interest

K Takeuchi is a consultant providing advisory services to Dako for their antibodies.

References

1 Lynch TJ, Bell DW, Sordella R, *et al.* Activating mutations in the epidermal growth factor receptor underlying responsiveness of non-small-cell lung cancer to gefitinib. N Engl J Med 2004;350:2129–2139.

2 Paez JG, Janne PA, Lee JC, *et al.* EGFR mutations in lung cancer: correlation with clinical response to gefitinib therapy. Science 2004;304:1497–1500.
3 Pao W, Miller V, Zakowski M, *et al.* EGF receptor gene mutations are common in lung cancers from 'never smokers' and are associated with sensitivity of tumors to gefitinib and erlotinib. Proc Natl Acad Sci USA 2004;101:13306–13311.
4 Shigematsu H, Lin L, Takahashi T, *et al.* Clinical and biological features associated with epidermal growth factor receptor gene mutations in lung cancers. J Natl Cancer Inst 2005;97:339–346.
5 Pfeifer GP, Denissenko MF, Olivier M, *et al.* Tobacco smoke carcinogens, DNA damage and p53 mutations in smoking-associated cancers. Oncogene 2002;21:7435–7451.
6 Suzuki H, Takahashi T, Kuroishi T, *et al.* p53 mutations in non-small cell lung cancer in Japan: association between mutations and smoking. Cancer Res 1992;52:734–736.
7 Soda M, Choi YL, Enomoto M, *et al.* Identification of the transforming EML4-ALK fusion gene in non-small-cell lung cancer. Nature 2007;448:561–566.
8 Choi YL, Takeuchi K, Soda M, *et al.* Identification of novel isoforms of the EML4-ALK transforming gene in non-small cell lung cancer. Cancer Res 2008;68:4971–4976.
9 Takeuchi K, Choi YL, Soda M, *et al.* Multiplex reverse transcription-PCR screening for EML4-ALK fusion transcripts. Clin Cancer Res 2008;14:6618–6624.
10 Rikova K, Guo A, Zeng Q, *et al.* Global survey of phosphotyrosine signaling identifies oncogenic kinases in lung cancer. Cell 2007;131:1190–1203.
11 Koivunen JP, Mermel C, Zejnullahu K, *et al.* EML4–ALK fusion gene and efficacy of an ALK kinase inhibitor in lung cancer. Clin Cancer Res 2008;14:4275–4283.
12 Inamura K, Takeuchi K, Togashi Y, *et al.* EML4-ALK fusion is linked to histological characteristics in a subset of lung cancers. J Thorac Oncol 2008;3:13–17.
13 Travis WD, Brambilla E, Muller-Hermelink HK, *et al.* World Health Organization Classification of Tumours: Pathology and Genetics of Tumours of the Lung, Pleural, Thymus and Heart. Springer: Berlin, 2004.
14 Japan Lung Cancer Society. General Rules for Clinical and Pathologic Record of Lung Cancer [in Japanese], 5th edn. Kanahara: Tokyo, 1999.
15 Inamura K, Satoh Y, Okumura S, *et al.* Pulmonary adenocarcinomas with enteric differentiation: histologic and immunohistochemical characteristics compared with metastatic colorectal cancers and usual pulmonary adenocarcinomas. Am J Surg Pathol 2005;29:660–665.
16 Takeuchi K, Choi YL, Togashi Y, *et al.* KIF5B-ALK, a novel fusion oncokinase identified by an immunohistochemistry-based diagnostic system for ALK-positive lung cancer. Clin Cancer Res 2009 (in press).
17 Inamura K, Togashi Y, Nomura K, *et al.* Up-regulation of PTEN at the transcriptional level is an adverse prognostic factor in female lung adenocarcinomas. Lung Cancer 2007;57:201–206.
18 Hashimoto T, Tokuchi Y, Hayashi M, *et al.* Different subtypes of human lung adenocarcinoma caused by different etiological factors. Evidence from p53 mutational spectra. Am J Pathol 2000;157: 2133–2141.
19 Stein H, Foss HD, Durkop H, *et al.* CD30(+) anaplastic large cell lymphoma: a review of its histopathologic, genetic, and clinical features. Blood 2000;96:3681–3695.
20 Kosaka T, Yatabe Y, Endoh H, *et al.* Mutations of the epidermal growth factor receptor gene in lung cancer: biological and clinical implications. Cancer Res 2004;64:8919–8923.
21 Noda N, Matsuzoe D, Konno T, *et al.* K-ras gene mutations in non-small cell lung cancer in Japanese. Oncol Rep 2001;8:889–892.
22 Yatabe Y, Kosaka T, Takahashi T, *et al.* EGFR mutation is specific for terminal respiratory unit type adenocarcinoma. Am J Surg Pathol 2005;29:633–639.
23 Shibata T, Hanada S, Kokubu A, *et al.* Gene expression profiling of epidermal growth factor receptor/KRAS pathway activation in lung adenocarcinoma. Cancer Sci 2007;98:985–991.
24 Tanaka H, Yanagisawa K, Shinjo K, *et al.* Lineage-specific dependency of lung adenocarcinomas on the lung development regulator TTF-1. Cancer Res 2007;67:6007–6011.

Genome-wide histone methylation profile for heart failure

Ruri Kaneda[1,2], Shuji Takada[1], Yoshihiro Yamashita[1], Young Lim Choi[1], Mutsuko Nonaka-Sarukawa[2], Manabu Soda[1], Yoshio Misawa[3], Tadashi Isomura[4], Kazuyuki Shimada[2] and Hiroyuki Mano[1,5,*]

Divisions of [1]Functional Genomics, Jichi Medical University, Tochigi 329-0498, Japan
[2]Cardiovascular Medicine, Jichi Medical University, Tochigi 329-0498, Japan
[3]Cardiovascular Surgery, Jichi Medical University, Tochigi 329-0498, Japan
[4]Hayama Heart Center, Kanagawa 240-0116, Japan
[5]CREST, Japan Science and Technology Agency, Saitama 332-0012, Japan

Epigenetic alterations are implicated in the development of cardiac hypertrophy and heart failure, but little is known of which epigenetic changes in which regions of the genome play such a role. We now show that trimethylation of histone H3 on lysine-4 (K4TM) or lysine-9 (K9TM) is markedly affected in cardiomyocytes in association with the development of heart failure in a rat disease model. High-throughput pyrosequencing performed with ChIP products for K4TM or K9TM prepared from human left ventricular tissue with retained or damaged function also revealed that protein-coding genes located in the vicinity of K4TM marks differ between functional and disabled myocytes, yet both sets of genes encode proteins that function in the same signal transduction pathways for cardiac function, indicative of differential K4TM marking during the development of heart failure. However, K9TM mark-profile was less dependent on the disease status compared to that of K4TM. Our data collectively reveal global epigenetic changes in cardiac myocytes associated with heart failure.

Introduction

A variety of conditions, including pressure or volume overload in the cardiovascular system and remodeling of the left ventricle of the heart after ischemic damage, result in heart failure, which is characterized by a reduction in contractile ability and a decrease in the number of viable myocytes in the heart (James *et al.* 2000). Treatment of heart failure remains problematic, and this condition is thus still one of the leading causes of human death (Braunwald 1997).

Epigenetic status has been linked to cardiac hypertrophy and heart failure. The histone acetyltransferase activity of CREB-binding protein (CBP) and p300 is thus required for the induction of hypertrophic changes in cardiac muscle cells by phenylephrine (Gusterson *et al.* 2003). Consistent with this observation, inhibition of histone deacetylase (HDAC) activity results in an increase in the size of cardiac muscle cells (Iezzi *et al.* 2004). Furthermore, HDACs of class II (HDAC4, -5, -7, and -9) suppress cardiac hypertrophy in part by binding to and inhibiting the activity of myocyte enhancer factor 2 (Zhang *et al.* 2002). Induction of the atrial natriuretic peptide gene is associated with acetylation of histones (H3 and H4) located in the 3′ untranslated region of the gene (Kuwahara *et al.* 2001). Histones bound to the β-myosin heavy chain gene have also been shown to be targeted by histone acetyltransferases in cardiomyocytes (Zhang *et al.* 2002). Moreover, dynamic regulation of other histone modifications has been demonstrated in cardiac myocytes (Illi *et al.* 2005; Bingham *et al.* 2007).

It remains to be established, however, (i) which epigenetic marks are dysregulated in association with heart failure *in vivo*, (ii) which regions of the human genome are susceptible to such epigenetic changes, and (iii) how epigenetic dysregulation affects the expression of protein-coding or other genes. To address these issues, we have now studied an animal model of congestive heart failure (CHF), the Dahl salt-sensitive rat (Rapp *et al.* 1989), and found that two histone modifications are markedly affected in cardiac myocytes during the development of CHF. We further confirmed our findings in human left ventricular (LV) myocytes with the use of chromatin immunoprecipitation

Communicated by: Kohei Miyazono
**Correspondence*: hmano@jichi.ac.jp

DOI: 10.1111/j.1365-2443.2008.01252.x

(ChIP) coupled to pyrosequencing. Our results have revealed dynamic histone modifications in the vicinity of a subset of protein-coding genes in the human genome, which directly participate in regulation of the contraction of cardiac myocytes.

Results

Histone modifications in the heart of Dahl rats

We prepared LV myocytes from Dahl salt-sensitive rats, which are genetically intolerant to excessive salt intake (Rapp *et al.* 1989). A high-sodium diet thus induces systemic hypertension and cardiac hypertrophy in Dahl rats within a few weeks. These changes are followed within a few months by the development of CHF and death. We isolated cardiac myocytes from rats with CHF (fed a high-sodium diet) as well as from age-matched animals with a normal heart (fed a low-sodium diet), and we subjected these cells to ChIP with antibodies to acetylated histone H3 (H3Ac), acetylated histone H4 (H4Ac), histone H3 dimethylated on lysine-4 (K4DM), histone H3 trimethylated on lysine-4 (K4TM), histone H3 dimethylated on lysine-9 (K9DM), histone H3 trimethylated on lysine-9 (K9TM), histone H4 trimethylated on lysine-20 (K20TM), or histone H3 dimethylated on lysine-27 (K27DM). The ChIP products as well as cRNA prepared from the normal or failed hearts were then individually subjected to hybridization with high-density oligonucleotide microarrays (Affymetrix Rat Genome 230 2.0 GeneChip) originally developed for expression profiling of rat genes.

Pearson's correlation coefficient for the signal intensity of all probe sets with a "Present" call (by Affymetrix GCOS software) in the normal heart ($n = 13\ 914$) was 0.873 in the cRNA hybridizations for normal and failed hearts (Fig. 1), indicative of a strong correlation in the expression level of most genes between the two samples. Consistent with this observation, the signal intensity for all probe sets with a positive value in the H3Ac ChIP products from the normal heart ($n = 12\ 027$) was highly correlated between these products from normal and failed hearts ($r = 0.724$). A similar strong correlation between the two groups was observed for H4Ac.

Unexpectedly, however, despite the strong correlation ($r = 0.856$) apparent for K4DM, only a weak negative correlation ($r = -0.097$) was detected for the K4TM mark between normal and failed hearts, indicative of marked differences in the associated gene sets. Similarly, although a strong correlation was observed for K9DM ($r = 0.558$), a weak negative correlation ($r = -0.251$) was apparent for K9TM. Hybridization levels were positively correlated between normal and failed hearts for K20TM and K27DM.

Thus, among the epigenetic marks examined, K4TM and K9TM were the histone modifications most affected in heart failure. Although differences in functional roles and genomic distributions between K4DM and K4TM have been described (Santos-Rosa *et al.* 2002; Bernstein *et al.* 2005), little has been known of such differential roles for the methylation level of lysine-9 of histone H3.

K4TM and K9TM profiles in the human heart

We next attempted to identify the genomic regions associated with the K4TM and K9TM marks in human cardiac myocytes. ChIP products for K4TM or K9TM were prepared from a mixture of LV tissue specimens from four individuals with retained pumping function [LV ejection fraction (EF) of 65.5 ± 7.6%, mean ± SD] or from four individuals with CHF (LVEF of 19.8 ± 5.7%) caused by dilated cardiomyopathy (Table 1). The ChIP

Table 1 Clinical characteristics of the subjects who provided specimens for the study

	Sample ID	Disease	Age (years)	Sex	LVEF (%)
HighEF	PM 8	HVD (MSR, ASR)	59	F	65
	PM12	HVD (MSR)	73	F	58
	PM13	HVD (MS)	55	F	76
	PM14	HVD (MS)	62	F	63
CHF	LV13	DCM	52	M	17
	LV14	DCM	55	M	25
	LV18	DCM	57	M	13
	LV20	DCM	64	F	24

HVD, heart valvular disease; MS(R), mitral stenosis (and regurgitation); ASR, aortic stenosis and regurgitation; DCM, dilated cardiomyopathy; F, female; M, male.

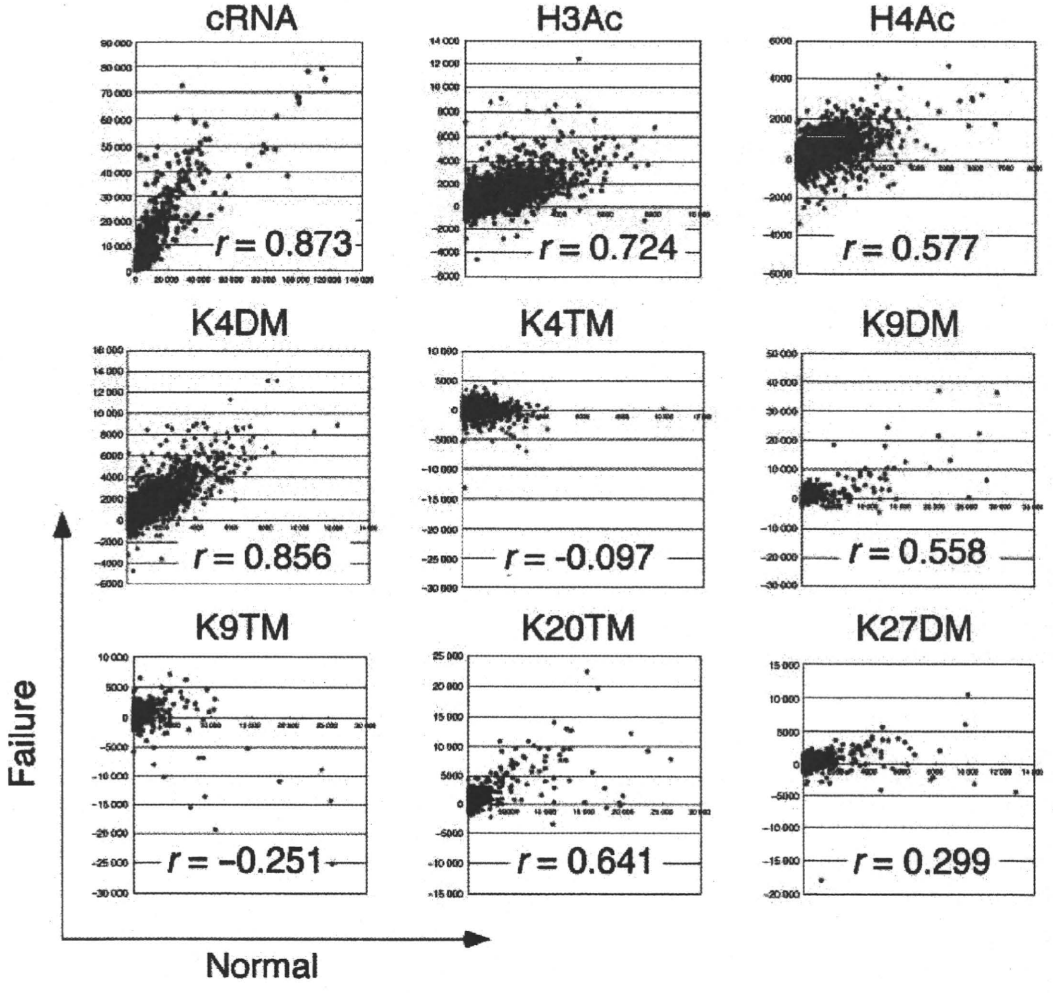

Figure 1 Comparison of epigenetic profiles between normal and failed rat hearts. The expression level of each probe set on oligonucleotide microarrays was compared between total cRNA from normal (*x* axis) or failed (*y* axis) hearts by calculation of Pearson's correlation coefficient (*r*). ChIP-on-chip data for H3Ac, H4Ac, K4DM, K4TM, K9DM, K9TM, K20TM, and K27DM are similarly compared.

products were subjected to pyrosequencing with the Genome Sequencer 20 system (Roche). In this "ChIP-to-seq" experiment, 96 069, 95 596, 116 267, and 96 734 reads were obtained for the K4TM products for specimens with retained LV ejection fraction (HighEF), the K4TM products for CHF, the K9TM products for HighEF, and the K9TM products for CHF, respectively. After quality-filtering, we isolated an average of 36 279 reads per sample, for each of which a single hit with a highest matching score was identified in the human genome sequence (the hg18 assembly of the Genome Bioinformatics Group, University of California at Santa Cruz) (Table S1 in Supporting Information). We thus focused on these reads for further analysis.

Many regions of the genome were identified in which multiple sequence reads mapped closely to each other. We therefore defined a "cluster" as a group of sequence reads localized within a distance of 1 kbp in the human genome (Fig. 2A). A total of 94 202 clusters was identified for all four samples, and 18 725 of these clusters, referred to as "high clusters," contained ≥ 2 sequence reads in ≥ 1 sample (see Table S2 in Supporting Information).

We then examined histone modification at the high clusters for specificity of the epigenetic mark (K4TM or

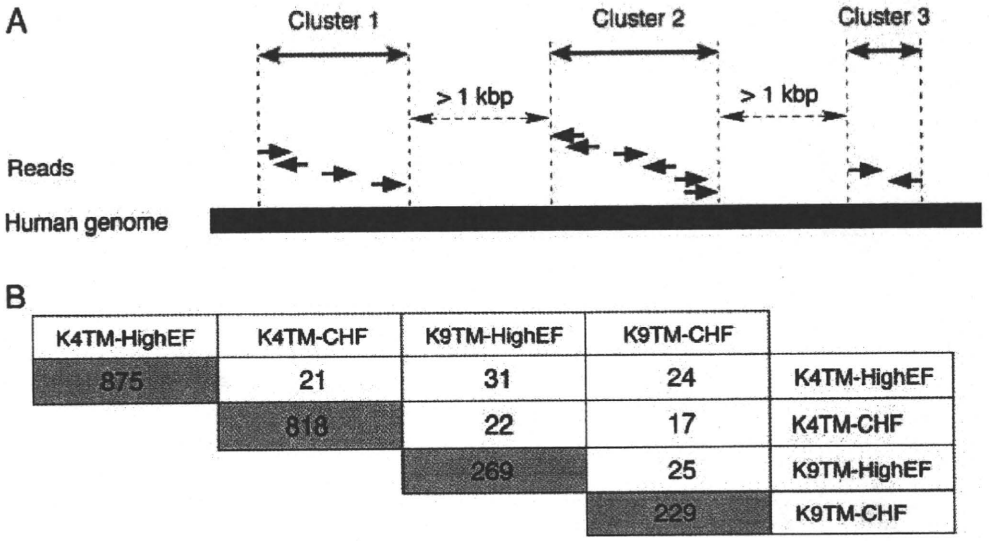

Figure 2 High clusters in K4TM and K9TM ChIP-to-seq data. (A) Groups of sequence reads that map to the human genome within a distance of 1 kbp are defined as "clusters," which are further denoted as "high clusters" when the read number in the cluster is ≥ 2 in ≥ 1 sample. (B) Numbers of high clusters with a read number of ≥ 5 for K4TM or K9TM in HighEF or CHF samples (shaded boxes). The numbers of such clusters shared between any pair of samples is also indicated (open boxes).

Table 2 Disease-specific high clusters

Mark	Characteristics of high clusters	Total number of high clusters	Number of high clusters close to RefSeq genes	Number of high clusters close to CpG islands
K4TM	HighEF ≥ 5, CHF ≤ 1	836	407	129
	HighEF ≤ 1, CHF ≥ 5	786	432	163
K9TM	HighEF ≥ 5, CHF ≤ 1	220	75	18
	HighEF ≤ 1, CHF ≥ 5	196	69	10

K9TM) and disease status (HighEF or CHF). Among the high clusters, 875 had ≥ 5 reads in the K4TM product for HighEF, 818 had ≥ 5 reads in the K4TM product for CHF, 269 had ≥ 5 reads in the K9TM product for HighEF, and 229 had ≥ 5 reads in the K9TM product for CHF (Fig. 2B). Only a few dozen of such high clusters were shared between any pair of samples, indicating the existence of disease-specific as well as methylation site-specific epigenetic profiles. Therefore, despite the heterogeneity in the cause of CHF (sustained systemic hypertension or dilated cardiomyopathy), both the Dahl rat and human data sets revealed a marked difference in the K4TM and K9TM epigenetic profiles between normal and failed hearts. Such specificity is further visualized for human chromosome 1 in Fig. S1 in Supporting Information. In contrast, the profile of read number per cluster was similar among the four groups of human ChIP products (see Fig. S2 in Supporting Information).

Genes mapped closely to disease-dependent clusters

We then isolated disease status-specific high clusters from the data set. A total of 836 high clusters was found to contain ≥ 5 reads in the K4TM products for HighEF but ≤ 1 read in those for CHF (HighEF-specific K4TM clusters); 407 RefSeq genes mapped to within ≤ 5 kbp of these clusters (Table 2). Similarly, 786 high clusters were found to be specific for K4TM and CHF (≤ 1 read in the K4TM products for HighEF but ≥ 5 reads in those for CHF). Smaller numbers of disease-dependent clusters were identified for the K9TM mark (220 HighEF-specific and 196 CHF-specific). These disease-dependent clusters

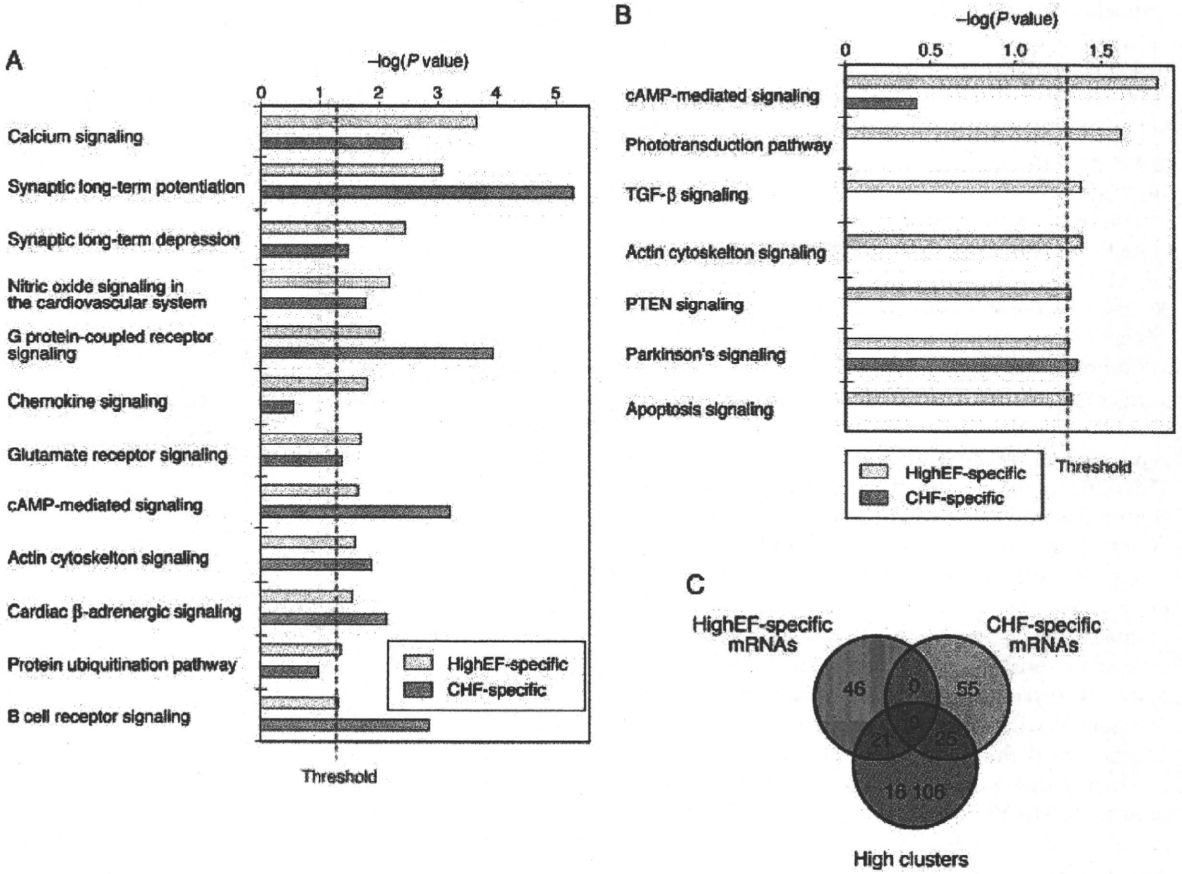

Figure 3 Analysis of genes that map in the vicinity of disease-dependent high clusters. (A) Canonical signaling pathways overrepresented in the HighEF-specific or CHF-specific high clusters for the K4TM ChIP products are listed with the corresponding −log(*P* value) score. (B) Canonical signaling pathways overrepresented in the HighEF-specific or CHF-specific high clusters for the K9TM ChIP products are listed with the corresponding −log(*P* value) score. (C) Venn diagram for comparison of transcripts associated specifically with HighEF or CHF status and those encoded by genes that map within a distance of < 5 kbp relative to a high cluster.

were widely distributed throughout human chromosomes and showed little overlap (see Fig. S3 in Supporting Information).

We examined whether the protein products of RefSeq genes that mapped in the vicinity (a distance of ≤ 5 kbp) of disease-dependent clusters function in canonical intracellular signaling pathways with the use of Ingenuity Pathway Analysis software (Ingenuity Systems; http://www.ingenuity.com). Analysis of the RefSeq genes associated with the disease-dependent K4TM clusters identified 12 canonical pathways that were significantly overrepresented ($P < 0.05$, Fisher's exact test) in HighEF-specific clusters and 20 pathways overrepresented in CHF-specific clusters. Many of the pathways ($n = 10$) were overrepresented in both HighEF-K4TM and CHF-K4TM clusters, almost all of which (including those for calcium signaling, synaptic long-term regulation, and nitric oxide signaling) are related to cardiac function (Fig. 3A).

Consistent with the disease-dependent selection of the clusters, the HighEF-associated and CHF-associated genes were distinct even within the same pathways. The canonical pathway for synaptic long-term potentiation, for example, contains the products of eight HighEF-associated and 12 CHF-associated genes, the interactions among which are shown in Fig. S4 in Supporting Information. Although genes corresponding to the calmodulin complex are present in both gene sets, these genes differ between the HighEF set (*CALM1*) and the CHF set (*CALM3*).

In addition to the proteins of the canonical signaling pathways, many products of the genes in the vicinity of disease-dependent high clusters for K4TM are functionally or physically networked. One such network comprises 34 proteins, 18 of which are encoded by HighEF-associated genes and 16 by CHF-associated genes (Fig. S5 in Supporting Information). Again, the genes for some complexes associated with both gene sets are distinct; those for the ATPase complex, for instance, include that for ATP1B1 in the HighEF-associated set and that for ATP5C1 in the CHF-associated set. Gene products in this network are substantially enriched in those implicated in cardiovascular disease.

In contrast to the K4TM-specific clusters, only a few canonical signaling pathways are linked to the RefSeq genes localized in the vicinity of K9TM-specific clusters. This difference is due in part to the small number of high clusters that contain disease-dependent reads for K9TM. Whereas the numbers of high clusters for HighEF specimens were similar between K4TM and K9TM products ($n = 6547$ and 5594, respectively), the numbers of disease-dependent clusters for the K9TM mark were only approximately 25% of those for the K4TM mark (Table 2). Seven canonical signaling pathways were over-represented ($P < 0.05$, Fisher's exact test) in the genes associated with the HighEF-K9TM clusters, whereas only one such pathway was overrepresented in those associated with the CHF-K9TM clusters (Fig. 3B). The network containing the most disease-dependent K9TM-associated gene products is centered on transforming growth factor β1 (TGFB1) and the tumor suppressor p53 (TP53), implicating K9TM-related regulation in cell death in the heart (see Fig. S6 in Supporting Information).

Our analysis thus revealed differential regulation of K4TM modification for genes related to cardiac function. To examine whether such epigenetic regulation plays a direct role in gene transcription, we performed gene expression profiling with Human Genome U133 Plus 2.0 arrays (Affymetrix) for the individual specimens (four for HighEF and four for CHF) used in the ChIP experiments. From the data obtained for 54 675 probe sets and the eight specimens, we selected HighEF-specific probe sets according to the following criteria: (i) the ratio of the mean expression level between HighEF and CHF was ≥ 3, and (ii) the mean expression level in HighEF was ≥ 10 arbitrary units (U). These criteria resulted in the isolation of 67 probe sets (see Table S3 in Supporting Information). CHF-specific probe sets were also selected on the basis of a CHF/HighEF ratio for mean expression level of ≥ 3 and a mean expression level in CHF of ≥ 10 U, resulting in the identification of 80 probe sets (see Table S4 in Supporting Information). A total of 16 152 of the transcripts measured with the U133 Plus 2.0 arrays mapped within a distance of ≤ 5 kbp relative to the high clusters. A Venn diagram revealed that only 21 probe sets were shared between the HighEF-specific and high cluster–associated transcripts, whereas 25 probe sets were shared between the CHF-specific and high cluster–associated transcripts (Fig. 3C). The K4TM mark has been found to map preferentially to the transcription start sites of active genes (Bernstein *et al.* 2005). Although a typical correlation between the K4TM modification and selective gene expression was apparent for a subset of genes (Fig. 4), our results suggest that this dynamic epigenetic regulation in the heart may not always directly participate in transcriptional regulation of neighboring genes.

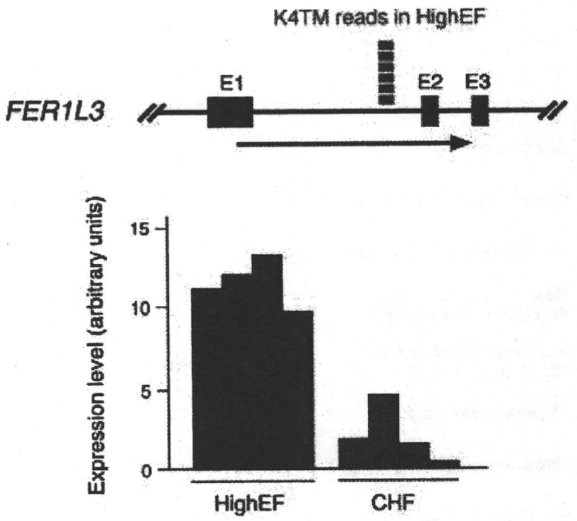

Figure 4 Epigenetic profile and mRNA abundance for *FER1L3*. Six sequence reads were selectively identified in the first intron of the *FER1L3* gene for the K4TM ChIP products of the HighEF sample (upper panel). E, exon. Consistent with this epigenetic profile, the amount of *FER1L3* mRNA was higher in the HighEF specimens than in the CHF specimens, as judged from the microarray data (lower panel).

Discussion

In the present study, we have revealed heart failure–dependent changes in the epigenetic profiles for K4TM and K9TM marks. The antibodies used in this study have been utilized in other reports for ChIP experiments, with those for K4TM and K9TM being especially employed in a genome-wide epigenetic profiling (Pokholok *et al.* 2005; Vakoc *et al.* 2006). Although it is difficult to

extensively verify our data in this study (because of the lack of knowledge in epigenetic profiles in heart), our ChIP procedure could faithfully confirm the epigenetic data demonstrated in previous studies [You *et al.* have, for instance, revealed that an apicidin treatment decreases the K4TM level while increases the K9TM level in the exon 1 of *DNMT1* in HeLa cells (You *et al.* 2008), and we could observe similar changes in the same experiment (data not shown)], supporting the reliability of our ChIP procedures.

Despite increasing evidence for a role of histone acetylation–deacetylation in the development of cardiac hypertrophy and heart failure, little information has been available for other histone modifications in these conditions (Illi *et al.* 2005; Phan *et al.* 2005; Bingham *et al.* 2007). Given the marked differences between the profiles of dimethylation and trimethylation for both K4 and K9 sites of histone H3, such trimethylation is likely under strict regulation in failed hearts.

The genes positioned close to the K4TM or K9TM marks were highly enriched in those that encode components of signaling pathways related to cardiac function. The HighEF-specific K4TM modification was, for instance, associated with *RYR2*, *CACNA2D1*, and *CACNB2* genes, the products of which directly participate in the regulation of intracellular calcium concentration and in muscle contraction (Cataldi *et al.* 1999; Marx *et al.* 2000). However, such disease-dependent histone methylation was not always linked to the induction or repression of neighboring genes. The expression level of the above three genes thus did not differ significantly between HighEF and CHF specimens (data not shown). Furthermore, only ~30% of HighEF- or CHF-specific transcripts were derived from genes associated with disease-dependent K4TM or K9TM modification (Fig. 3C). Consistent with such observations, the expression ratio for probe sets between normal and failed hearts of Dahl rats was not significantly correlated with the intensity ratio for any of the examined histone modifications, including H3Ac and H4Ac (data not shown). Therefore, despite the marked association between disease status and both transcript abundance and a subset of histone modifications, none of the latter can directly account for the former.

The epigenetic changes associated with heart failure may regulate gene transcription not through a single modification but through a combination of various marks (the "histone code" hypothesis) (Strahl & Allis 2000). The disease-dependent epigenetic changes also may alter the conformation of chromosomes, inducing an open or closed chromatin structure that indirectly affects the targets of subsequent regulation, such as the binding of transcription factors or additional chromatin remodeling. The subsequent regulation step would then play an important role in transcription of neighboring genes. In either case, our epigenetic profiles should facilitate further investigations into the roles of epigenetic changes in the development of heart failure.

Experimental procedures

ChIP-on-chip experiments

Dahl salt-sensitive rats (Japan SLC) at 6 weeks of age were maintained on a low-sodium diet (0.3% NaCl) or switched to a high-sodium diet (8% NaCl); the latter animals developed heart failure, as detected by echocardiography, after 13 weeks, as described previously (Ueno *et al.* 2003). ChIP products were prepared from the LV myocytes of 19-week-old Dahl rats with antibodies specific to H3Ac (Upstate, #17-245), H4Ac (Upstate, #17-229), K4DM (Abcam, #ab7766), K4TM (Abcam, #ab8580), K9DM (Upstate, #07-441), K9TM (Upstate, #07-442), K20TM (Abcam, #ab9053) or K27DM (Upstate, #07-452). The products were amplified by T7 RNA polymerase and subjected to hybridization with Affymetrix Rat Genome 230 2.0 microarrays as described previously (Takayama *et al.* 2007). Total genomic DNA (Pre-ChIP) and cRNA prepared from the LV tissue were also hybridized to the same arrays. The mean expression intensity of all probe sets was set to 500 U in each hybridization, and the fluorescence intensity of each test gene was normalized accordingly. Microarray data for rat and human hearts are available at the Gene Expression Omnibus web site (http://www.ncbi.nlm.nih.gov/geo) under the accession numbers GSE8341 and GSE8331, respectively. For the ChIP data, the signal intensity of each probe set in the Pre-ChIP analysis was then subtracted from that of the corresponding probe set in each ChIP experiment.

ChIP-to-seq experiments

All clinical specimens were obtained with written informed consent, and the study was approved by the ethics committees of Jichi Medical University and Hayama Heart Center. ChIP products were prepared from pooled samples for HighEF or CHF (each derived from four specimens) with antibodies to K4TM or K9TM. The products were converted to cRNA and amplified as described above for ChIP-on-chip experiments. The cRNA was then used to generate double-stranded DNA, which was subjected to pyrosequencing with a Genome Sequencer 20 system (Roche Diagnostics). Keypass wells occupied 82.7% to 87.0% of original Raw wells. Homology searches with the BLAST program were performed against the human genome sequence (the hg18 assembly) for each readout with the following parameter set: –e 2e-19 –v 50 –b 500 –T F –F F –m 8.

Acknowledgements

This work was supported in part by a Grant-in-Aid for Scientific Research on Priority Areas (C) "Medical Genome Science" from the

Ministry of Education, Culture, Sports, Science and Technology of Japan and by a grant (#04C7) from Salt Science Research Foundation (Tokyo, Japan).

References

Bernstein, B.E., Kamal, M., Lindblad-Toh, K., Bekiranov, S., Bailey, D.K., Huebert, D.J., McMahon, S., Karlsson, E.K., Kulbokas, E.J. 3rd, Gingeras, T.R., Schreiber, S.L. & Lander, E.S. (2005) Genomic maps and comparative analysis of histone modifications in human and mouse. *Cell* **120**, 169–181.

Bingham, A.J., Ooi, L., Kozera, L., White, E. & Wood, I.C. (2007) The repressor element 1-silencing transcription factor regulates heart-specific gene expression using multiple chromatin-modifying complexes. *Mol. Cell. Biol.* **27**, 4082–4092.

Braunwald, E. (1997) Shattuck lecture—cardiovascular medicine at the turn of the millennium: triumphs, concerns, and opportunities. *N. Engl. J. Med.* **337**, 1360–1369.

Cataldi, M., Secondo, A., D'Alessio, A., Taglialatela, M., Hofmann, F., Klugbauer, N., Di Renzo, G. & Annunziato, L. (1999) Studies on maitotoxin-induced intracellular $Ca^{(2+)}$ elevation in Chinese hamster ovary cells stably transfected with cDNAs encoding for L-type $Ca^{(2+)}$ channel subunits. *J. Pharmacol. Exp. Ther.* **290**, 725–730.

Gusterson, R.J., Jazrawi, E., Adcock, I.M. & Latchman, D.S. (2003) The transcriptional co-activators CREB-binding protein (CBP) and p300 play a critical role in cardiac hypertrophy that is dependent on their histone acetyltransferase activity. *J. Biol. Chem.* **278**, 6838–6847.

Iezzi, S., Di Padova, M., Serra, C., Caretti, G., Simone, C., Maklan, E., Minetti, G., Zhao, P., Hoffman, E.P., Puri, P.L. & Sartorelli, V. (2004) Deacetylase inhibitors increase muscle cell size by promoting myoblast recruitment and fusion through induction of follistatin. *Dev. Cell* **6**, 673–684.

Illi, B., Scopece, A., Nanni, S., Farsetti, A., Morgante, L., Biglioli, P., Capogrossi, M.C. & Gaetano, C. (2005) Epigenetic histone modification and cardiovascular lineage programming in mouse embryonic stem cells exposed to laminar shear stress. *Circ. Res.* **96**, 501–508.

James, M.A., Saadeh, A.M. & Jones, J.V. (2000) Wall stress and hypertension. *J. Cardiovasc. Risk* **7**, 187–190.

Kuwahara, K., Saito, Y., Ogawa, E., Takahashi, N., Nakagawa, Y., Naruse, Y., Harada, M., Hamanaka, I., Izumi, T., Miyamoto, Y., Kishimoto, I., Kawakami, R., Nakanishi, M., Mori, N. & Nakao, K. (2001) The neuron-restrictive silencer element-neuron-restrictive silencer factor system regulates basal and endothelin 1-inducible atrial natriuretic peptide gene expression in ventricular myocytes. *Mol. Cell. Biol.* **21**, 2085–2097.

Marx, S.O., Reiken, S., Hisamatsu, Y., Jayaraman, T., Burkhoff, D., Rosemblit, N. & Marks, A.R. (2000) PKA phosphorylation dissociates FKBP12.6 from the calcium release channel (ryanodine receptor): defective regulation in failing hearts. *Cell* **101**, 365–376.

Phan, D., Rasmussen, T.L., Nakagawa, O., McAnally, J., Gottlieb, P.D., Tucker, P.W., Richardson, J.A., Bassel-Duby, R. & Olson, E.N. (2005) BOP, a regulator of right ventricular heart development, is a direct transcriptional target of MEF2C in the developing heart. *Development* **132**, 2669–2678.

Pokholok, D.K., Harbison, C.T., Levine, S., Cole, M., Hannett, N.M., Lee, T.I., Bell, G.W., Walker, K., Rolfe, P.A., Herbolsheimer, E., Zeitlinger, J., Lewitter, F., Gifford, D.K. & Young, R.A. (2005) Genome-wide map of nucleosome acetylation and methylation in yeast. *Cell* **122**, 517–527.

Rapp, J.P., Wang, S.M. & Dene, H. (1989) A genetic polymorphism in the renin gene of Dahl rats cosegregates with blood pressure. *Science* **243**, 542–544.

Santos-Rosa, H., Schneider, R., Bannister, A.J., Sherriff, J., Bernstein, B.E., Emre, N.C., Schreiber, S.L., Mellor, J. & Kouzarides, T. (2002) Active genes are tri-methylated at K4 of histone H3. *Nature* **419**, 407–411.

Strahl, B.D. & Allis, C.D. (2000) The language of covalent histone modifications. *Nature* **403**, 41–45.

Takayama, K., Kaneshiro, K., Tsutsumi, S., Horie-Inoue, K., Ikeda, K., Urano, T., Ijichi, N., Ouchi, Y., Shirahige, K., Aburatani, H. & Inoue, S. (2007) Identification of novel androgen response genes in prostate cancer cells by coupling chromatin immunoprecipitation and genomic microarray analysis. *Oncogene* **26**, 4453–4463.

Ueno, S., Ohki, R., Hashimoto, T., Takizawa, T., Takeuchi, K., Yamashita, Y., Ota, J., Choi, Y.L., Wada, T., Koinuma, K., Yamamoto, K., Ikeda, U., Shimada, K. & Mano, H. (2003) DNA microarray analysis of *in vivo* progression mechanism of heart failure. *Biochem. Biophys. Res. Commun.* **307**, 771–777.

Vakoc, C.R., Sachdeva, M.M., Wang, H. & Blobel, G.A. (2006) Profile of histone lysine methylation across transcribed mammalian chromatin. *Mol. Cell. Biol.* **26**, 9185–9195.

You, J.S., Kang, J.K., Lee, E.K., Lee, J.C., Lee, S.H., Jeon, Y.J., Koh, D.H., Ahn, S.H., Seo, D.W., Lee, H.Y., Cho, E.J. & Han, J.W. (2008) Histone deacetylase inhibitor apicidin downregulates DNA methyltransferase 1 expression and induces repressive histone modifications via recruitment of corepressor complex to promoter region in human cervix cancer cells. *Oncogene* **27**, 1376–1386.

Zhang, C.L., McKinsey, T.A., Chang, S., Antos, C.L., Hill, J.A. & Olson, E.N. (2002) Class II histone deacetylases act as signal-responsive repressors of cardiac hypertrophy. *Cell* **110**, 479–488.

Received: 26 June 2008
Accepted: 10 October 2008

Supporting Information/Supplementary materials

The following Supporting Information can be found in the online version of the article:

Figure S1 Distribution of K4TM and K9TM marks on chromosome 1.

Figure S2 Distribution of read number per cluster in ChIP products.

Figure S3 Chromosome distribution of disease-specific high clusters.

Figure S4 Protein complexes in the synaptic long-term potentiation pathway in Fig. 3A are colored red or green on the basis of whether the corresponding genes are associated with HighEF-specific or CHF-specific high clusters for K4TM, respectively.

Figure S5 Interaction map for a protein network that contains the products of 18 and 16 genes associated with the HighEF-specific and CHF-specific high clusters for K4TM, respectively.

Figure S6 Network for the products of genes that mapped in the vicinity of K9TM high clusters.

Table S1 Output of pyrosequencing.

Table S2 High clusters identified in the heart specimens.

Table S3 Expression intensity of HighEF-specific probe sets.

Table S4 Expression intensity of CHF-specific probe sets.

Additional Supporting Information may be found in the online version of the article.

Please note: Wiley-Blackwell are not responsible for the content or functionality of any supporting information supplied by the authors. Any queries (other than missing material) should be directed to the corresponding author for the article.

Potential role of miR-29b in modulation of *Dnmt3a* and *Dnmt3b* expression in primordial germ cells of female mouse embryos

SHUJI TAKADA,[1,4] EUGENE BEREZIKOV,[2] YOUNG LIM CHOI,[1] YOSHIHIRO YAMASHITA,[1] and HIROYUKI MANO[1,3]

[1]Division of Functional Genomics, Jichi Medical University, 3311-1 Yakushiji, Shimotsukeshi, Tochigi 329-0498, Japan
[2]Hubrecht Institute, Uppsalalaan 8, Utrecht, The Netherlands
[3]Core Research for Evolution Science and Technology (CREST), Japan Science and Technology Agency, Saitama 332-0012, Japan

ABSTRACT

MicroRNAs (miRNAs) are a recently discovered class of small noncoding RNAs and are implicated in an increasing number of biological processes. To examine whether miRNAs might contribute to sexual differentiation, we performed expression profiling of miRNAs in mouse embryonic gonads with the use of a highly sensitive cloning method, mRAP. Our profiling data revealed substantial differences in the miRNA repertoire between male and female gonads at embryonic (E) day 13.5 (E13.5), suggesting that such differentially expressed miRNAs may function in sexual differentiation. Female-specific miRNAs included miR-29b, which also has been known to be expressed in a similar sex-dependent manner in the gonads of chicken embryos, suggestive of a conserved role in gonadogenesis. Transcripts of the human genes for the de novo methyltransferases DNMT3A and DNMT3B have been identified as targets of miR-29b, and we found that mouse miR-29b also negatively regulates *Dnmt3a* and *Dnmt3b* expression in luciferase reporter assays. We also found that miR-29b is expressed in mouse primordial germ cells (PGCs) at E13.5 and that its expression is up-regulated in a female-specific manner between E13.5 and E17.5, when male-specific de novo methylation of the PGC genome is known to occur. Our data thus suggest that miR-29b may play an important role in female gonadal development by targeting *Dnmt3a* and *Dnmt3b* and thereby modulating methylation of genomic DNA in PGCs.

Keywords: mRAP; microRNA; mouse; chicken; gonad; primordial germ cell

INTRODUCTION

MicroRNAs (miRNAs) are short noncoding RNAs of 20–24 nucleotides (nt) that negatively regulate protein production from target mRNAs. They function by interacting with their target mRNAs through incomplete base-pairing to the 3′ untranslated region (3′UTR) (Filipowicz 2005; Hammond 2005; Hannon 2002; Mattick and Makunin 2005) and thereby either trigger degradation of the target mRNAs or suppress their translation. MicroRNAs have been identified in a wide range of organisms, including plants and animals (Carrington and Ambros 2003; Bartel 2004). Many miRNAs are conserved throughout evolution, but substantial diversity is also apparent for some miRNAs even between closely related species (Berezikov et al. 2006a).

Expression of miRNAs has been shown to be tightly regulated in a developmental stage-dependent, as well as in an organ-dependent, manner (Aboobaker et al. 2005; Wienholds et al. 2005; Ason et al. 2006; Kloosterman et al. 2006; Takada et al. 2006a), suggesting that they may play important roles in embryonic development and tissue organization. The miRNAs miR-1 and miR-124, for example, are specifically expressed in muscle and the central nervous system, respectively, in zebrafish, medaka, mouse, and fly, suggesting that the function of these miRNAs is conserved across animal phyla (Kloosterman and Plasterk 2006).

Although the precise function of most miRNAs remains unclear, some have been shown to contribute to a variety of biological phenomena, including intracellular signaling, apoptosis, metabolism, cardiogenesis, myogenesis, and brain development (Kloosterman and Plasterk 2006). Essential roles for miRNAs in animal development have been revealed

[4]**Present address:** Department of Systems BioMedicine, National Institute for Child Health and Development, 2-10-1 Okura, Setagaya, Tokyo, Japan 157-8535.

Reprint requests to: Shuji Takada, Department of Systems BioMedicine, National Institute for Child Health and Development, 2-10-1 Okura, Setagaya, Tokyo, Japan 157-8535; e-mail: stakada@nch.go.jp; fax: 81-3-3417-2498.

Article published online ahead of print. Article and publication date are at http://www.rnajournal.org/cgi/doi/10.1261/rna.1418309.

by analysis of cells deficient in Dicer, an enzyme required for the production of miRNAs from their precursors. *Dicer* null mutant mice thus die in utero at embryonic (E) day 7.5 (E7.5) and lack stem cell compartments (Bernstein et al. 2003). Mice with conditional ablation of this gene have also revealed that Dicer (and, therefore, probably also miRNAs) is required for morphogenesis of the limb (Harfe et al. 2005), skin (Andl et al. 2006; Yi et al. 2006), and lung epithelium (Harris et al. 2006). However, the genes targeted by miRNAs to achieve their effects remain largely unknown.

The heterogametic pairing of the sex chromosomes, X and Y, results in male development in mammals, whereas females are the heterogametic sex (ZW) in birds. Despite this difference in sex determination, several important genes for sexual differentiation are expressed in a similar manner in the gonads of both mammals and birds, suggesting the existence of a shared mechanism for this process. In mammals, the gonads first emerge as bipotential organs that subsequently develop into testes or ovaries depending on whether *Sry*, a sex-determining gene on the Y chromosome, is expressed or not (Gubbay et al. 1990; Koopman et al. 1991).

Identification of a function for miRNAs in mammalian gonadal development would be facilitated by characterization of miRNA expression profiles in developing gonads. However, most current technologies for measurement of miRNA expression either require substantial amounts of RNA for analysis (in the case of conventional cloning methods) or are unable to examine unknown miRNA species (in the case of microarray- or stem–loop-based detection methods). Neither of these types of approach is, therefore, suitable for extensive miRNA profiling of the gonads, for which only small quantities of tissue are usually available and many unknown miRNAs may be present.

We have recently developed a highly sensitive cloning procedure for miRNAs (Mano and Takada 2007; Takada et al. 2006a; Takada and Mano 2007). This procedure, designated miRNA amplification profiling (mRAP), allows the isolation of tens of thousands of miRNA clones from small quantities of starting material (even from as few as 10,000 cells). Coupling of mRAP to a computational pipeline in order to detect or predict miRNAs thus represents an optimal means for quantitative measurement of miRNA expression profiles in small amounts of tissue or clinical specimens. We have now applied such technology to mouse gonads in order to identify sex-dependent expression of miRNAs.

RESULTS

miRNA expression profiling of mouse embryonic gonads

To identify miRNAs expressed differentially between male and female mouse gonads at E13.5, we constructed small RNA-derived cDNA libraries by the mRAP protocol from these tissues. Totals of 672 and 1440 cDNA concatamers were sequenced, resulting in the identification of 1153 and 1480 small RNA sequences, for male and female embryonic gonads, respectively. Totals of 180 and 184 of these sequences from male and female gonad libraries, respectively, matched known miRNAs (Table 1). In addition, three candidates for novel miRNAs (miR-143*, miR-715*, miR-689*) were identified, each of which is present in the hairpin structure of known miRNAs. The remaining small RNA sequences likely represent RNA degradation products.

Identification of miRNAs that are expressed in a sex-dependent manner at E13.5

We have previously shown that mRAP cloning frequency reflects relative miRNA abundance in cells, provided that sufficient numbers of small RNA-derived cDNAs are sequenced (Takada et al. 2006a; S Takada and H Mano, unpubl.). In the current data set, many miRNAs were found to be expressed in a sex-dependent manner. For instance, the most abundant miRNA in both sexes, miR-29b, is preferentially expressed (by a factor of ~2) in the female gonad (Table 1).

To confirm such sexually differential expression of miRNAs, we performed Northern blot analysis. The abundance of miR-29b normalized by that of U6 RNA was 2.3 arbitrary units (U) in the female gonad and 1.0 U in the male gonad at E13.5 (Fig. 1), consistent with the mRAP data (read counts of 73.0% and 30.4% for female and male, respectively) (Table 1). In contrast, the fourth most abundant miRNA, miR-143, was found to be preferentially expressed in male gonads by both Northern blot analysis (1.7 versus 1.0 U in male and female, respectively) (Fig. 1) and mRAP analysis (8.70% versus 0.51%) (Table 1), although the male-to-female ratio differed between the two approaches. The sex-related expression of other miRNAs (miR-24, miR-142-3p, miR-126-5p) revealed by mRAP was not detected by Northern analysis (Fig. 1). Together, these data thus showed that certain miRNAs are expressed in the gonads in a sex-dependent manner.

Expression patterns of miR-29b and miR-143 during sexual differentiation

With the use of Northern blot analysis, we next examined the expression profiles of the sex-specific miRNAs miR-29b and miR-143 during mouse gonadogenesis. In the female gonad, expression of miR-29b was increased at E15.5 compared with that at E13.5, and the increased level of expression was maintained through E17.5 (Fig. 2). In the male gonad, the relative abundance of miR-29b increased gradually from E13.5 to E17.5 but was consistently lower than that in stage-matched female gonads, suggesting that miR-29b may play different roles in male and female gonads.

TABLE 1. Profiling of miRNAs by mRAP in mouse embryonic gonads at E13.5

miRNA	Read counts (%)[a] Male	Female
mmu-mir-29b	56 (30.43)	143 (72.96)
mmu-mir-142-3p	28 (15.22)	8 (4.08)
mmu-mir-124	14 (7.61)	5 (2.55)
mmu-mir-143	16 (8.70)	1 (0.51)
mmu-mir-689	1 (0.54)	11 (5.61)
mmu-mir-24	9 (4.89)	1 (0.51)
mmu-mir-1	5 (2.72)	2 (1.02)
mmu-mir-126-5p	4 (2.17)	1 (0.51)
mmu-let-7c	3 (1.63)	1 (0.51)
mmu-mir-142-5p	2 (1.09)	2 (1.02)
mmu-let-7b	1 (0.54)	3 (1.53)
mmu-mir-143*	4 (2.17)	0 (0)
mmu-mir-19b	2 (1.09)	2 (1.02)
mmu-mir-191	3 (1.63)	0 (0)
mmu-mir-146a	1 (0.54)	2 (1.02)
mmu-mir-351	3 (1.63)	0 (0)
mmu-let-7g	2 (1.09)	0 (0)
mmu-mir-541	2 (1.09)	0 (0)
mmu-mir-194	2 (1.09)	0 (0)
mmu-mir-126-3p	2 (1.09)	0 (0)
mmu-mir-30c	2 (1.09)	0 (0)
mmu-mir-130a	1 (0.54)	1 (0.51)
mmu-mir-217	2 (1.09)	0 (0)
mmu-mir-145	1 (0.54)	1 (0.51)
mmu-mir-99b	1 (0.54)	1 (0.51)
mmu-mir-30b	2 (1.09)	0 (0)
mmu-mir-28*	0 (0)	2 (1.02)
mmu-mir-141	2 (1.09)	0 (0)
mmu-mir-715*	0 (0)	1 (0.51)
mmu-mir-223	1 (0.54)	0 (0)
mmu-mir-136*	0 (0)	1 (0.51)
mmu-mir-29c	1 (0.54)	0 (0)
mmu-mir-19a	0 (0)	1 (0.51)
mmu-mir-184	1 (0.54)	0 (0)
mmu-mir-27b	1 (0.54)	0 (0)
mmu-mir-27a	1 (0.54)	0 (0)
mmu-mir-301a	0 (0)	1 (0.51)
mmu-mir-715	0 (0)	1 (0.51)
mmu-mir-298	0 (0)	1 (0.51)
mmu-mir-30a	1 (0.54)	0 (0)
mmu-mir-378	1 (0.54)	0 (0)
mmu-mir-744	1 (0.54)	0 (0)
mmu-mir-33	0 (0)	1 (0.51)
mmu-mir-125a-5p	1 (0.54)	0 (0)
mmu-mir-125b-5p	1 (0.54)	0 (0)
mmu-mir-139-5p	1 (0.54)	0 (0)
mmu-mir-92a	1 (0.54)	0 (0)
mmu-mir-214	1 (0.54)	0 (0)
mmu-mir-122	0 (0)	1 (0.51)
mmu-mir-689*	0 (0)	1 (0.51)
Total	184 (100)	196 (100)

[a]Cloning frequency of each miRNA in the library was expressed as a percentage of the total counts for all miRNA reads in each organ.

The expression of miR-143 in the male gonad increased from E13.5 to E15.5 but decreased to an intermediate level at E17.5 (Fig. 2). In contrast, the relative amount of miR-143 increased gradually between E13.5 and E17.5 in the female gonad, suggesting that this miRNA might have a specific function in male gonadogenesis at E15.5.

Evolutionary conservation of miR-29b and miR-143 expression

If miR-29b or miR-143 contributes directly to sex-dependent differentiation of the gonads in mice, their expression profiles might be expected to be evolutionarily conserved. This has been, indeed, shown in the cases for *Sox9*, *Amh*, and *FoxL2*, all of which are essential for sexual differentiation of the gonads (Carre-Eusebe et al. 1996; Kent et al. 1996; Morais da Silva et al. 1996; Loffler et al. 2003). We therefore examined the expression of miR-29b and miR-143 in chicken embryonic gonads during sexual differentiation with Northern blot analysis using male and female chicken embryonic gonads. The right and left gonads were treated separately, because there is a left–right asymmetry associated with the chicken gonadal differentiation. The relative abundance of miR-29b was greater in female gonads than in male gonads of chicken embryos at days 12 and 18 (Fig. 3), an expression profile similar to that apparent for mouse gonads (Fig. 2). In contrast, the expression of miR-143 was greater in male than in female chicken gonads at day 18 (Fig. 3). The preferential expression of miR-143 in male gonads was thus confirmed in chicken in a similar pattern to that in mouse (Fig. 2).

Identification of cell types in which miR-29b and miR-143 are expressed

We next investigated which cells express miR-29b or miR-143 in the gonads of mouse embryos. To determine

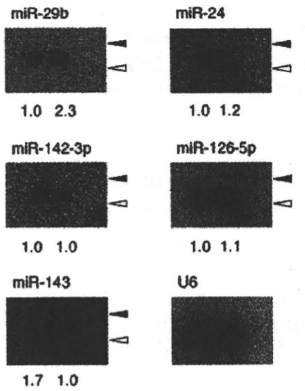

FIGURE 1. Validation of mRAP data by Northern blot analysis. Fractions containing small RNAs (0.5–0.8 μg per lane) isolated from (*left* lanes) male or (*right* lanes) female mouse gonads at E13.5 were subjected to Northern analysis with LNA probes specific for the indicated miRNAs or U6 RNA. The signal intensity for each miRNA normalized by that of U6 RNA is shown at the *bottom* of each lane. (Closed and open arrowheads) The positions corresponding to 24 and 19 nt, respectively.

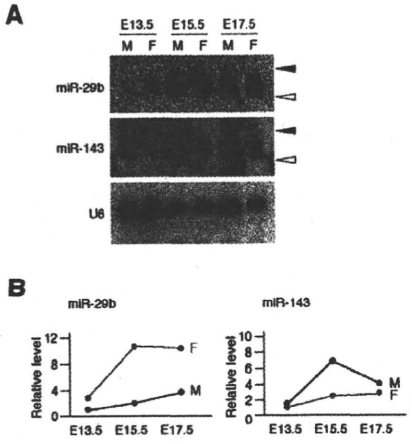

FIGURE 2. Sex-dependent expression profiles of miR-29b and miR-143 in mouse embryos. (*A*) Fractions containing small RNAs isolated from male (M) or female (F) mouse gonads at E13.5, E15.5, or E17.5 were subjected to Northern blot analysis with probes specific for miR-29b, miR-143, or U6 RNA. (Closed and open arrowheads) The positions corresponding to 24 and 19 nt, respectively. (*B*) The hybridization signal intensity for each miRNA in *A* was normalized by that of U6 RNA and plotted against embryonic stage.

whether such expression is restricted to somatic or germ cells, we performed Northern blot analysis with RNA isolated from embryos exposed in utero to busulfan, which is known to eliminate germ cells (Forsberg and Olivecrona 1966). Depletion of germ cells in busulfan-treated mouse gonads was confirmed by measurement of the expression of *Oct4* that is restricted to primordial germ cells (PGCs) in both testis and ovary at E13.5 (Pesce et al. 1998). Whole-mount in situ hybridization thus revealed the presence of *Oct4* mRNA in E13.5 mouse gonads exposed to DMSO vehicle but not in those exposed to busulfan (Fig. 4A).

Northern blot analysis with an LNA probe for miR-29b detected a discrete signal with RNA recovered from DMSO-treated female gonads, whereas the signal was mostly lost with RNA from those treated with busulfan (Fig. 4B), indicating that miR-29b is expressed exclusively in PGCs in female embryonic gonads. Although miR-143 was also found to be preferentially expressed in PGCs, a substantial amount of this miRNA remained in busulfan-treated male gonads, suggesting that miR-143 may be expressed in both somatic cells and PGCs of the testis.

Target genes of miR-29b in mouse PGCs

Our findings that miR-29b is expressed almost exclusively in PGCs of female gonads and that the expression profile of this miRNA is conserved between mouse and chicken suggests that miR-29b function is likely important for PGCs in female gonads. The genes for DNA methyltransferases 3A (DNMT3A) and 3B (DNMT3B) were recently shown to be direct targets of miR-29b, and overexpression of this miRNA results in a reduction in the global level of DNA methylation in the human genome (Fabbri et al. 2007). Given that mouse *Dnmt3a* and *Dnmt3b* are expressed in PGCs at E12.5–E17.5 (Lees-Murdock et al. 2005), these genes are candidates for regulation by miR-29b in mouse PGCs. Indeed, the TargetScan program (Lewis et al. 2003; Grimson et al. 2007), an in silico approach to the prediction of miRNA targets, indicated that both *Dnmt3a* and *Dnmt3b* are potential targets of this mouse miRNA (Fig. 5A). We, therefore, examined whether *Dnmt3a* or *Dnmt3b* is regulated by miR-29b in mouse.

To this end, we utilized a luciferase reporter assay. As a host cell line, using Northern blot analysis we searched for a cell line in which miR-29b does not exist; however, such a cell line was not found (data not shown). Since transfection efficiency of NIH3T3 is high, we used this cell line as a host cell. DNA fragments corresponding to portions of the 3′UTRs of *Dnmt3a* or *Dnmt3b* mRNAs containing the predicted miR-29b target sites were inserted into the 3′UTR of firefly luciferase cDNA, and the resulting reporter plasmids were introduced with or without miR-29b into NIH3T3 fibroblasts. The same target sequences but with a 1-base-pair (bp) mismatch were similarly inserted into the luciferase cDNA to yield negative control constructs (Fig. 5A). The luciferase activities of the constructs with the wild-type target regions of *Dnmt3a* or *Dnmt3b* were reduced compared with those of the corresponding mutant

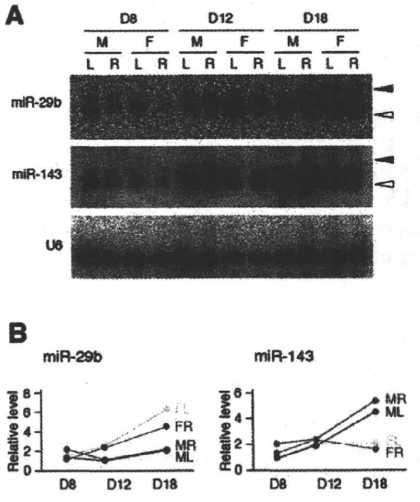

FIGURE 3. Sex-specific up-regulation of miR-29b and miR-143 expression in chicken embryos. (*A*) Fractions containing small RNAs isolated from male (M) or female (F) chicken gonads at day (D) 8, 12, or 18 were subjected to Northern blot analysis with probes specific for miR-29b, miR-143, or U6 RNA. (L) Left gonad; (R) right gonad. (Closed and open arrowheads) The positions corresponding to 24 and 19 nt, respectively. (*B*) The hybridization signal intensity for each miRNA in *A* was normalized by that of U6 RNA and plotted against embryonic stage. (ML) Male left gonad; (MR) male right gonad; (FL) female left gonad; (FR) female right gonads.